國立雲林科技大學
99 學年度博士班招生考試試題

所別：工程科技研究所
科目：計算機演算法

1. (10 points) (a)Compare the differences between the the Kruskal algorithm and the Prim algorithm.

   (10 points) (b)Use the Kruskal algorithm or the Prim's algorithm to find a minimum spanning tree of the following graph. **Note that you must point out what algorim is used to solve the problem and you must show your solution step by step. No point is given if you show the answer directly.**

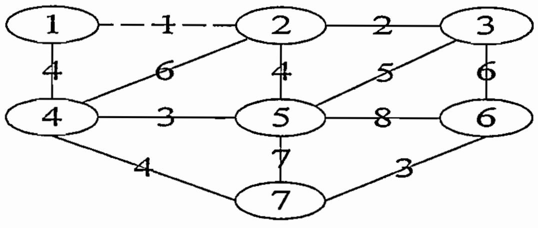

2. (30 points) The following statements are incorrect, **point out and correct** the errors in each of them.
   (a) Binary search uses the divide-and-conquer strategy.
   (b) QuickSort uses the divide-and-conquer strategy and "Divide in constant time, merge in O(n) time".
   (c) Depth-First-Search uses the queue data strucute.
   (d) The solution of the following recurrence: T(n)=2T(n/2)+O(n)+O(nlog n) is O(n).
   (e) The median finding problem can be done in O(n) by using the dynamic programming approach.
   (f) If a problem is NP-complete, its special cases are NP-complete.
   (g) Traveling salesperson problem and One Center problem are NP-complete.
   (h) A problem is easy if it can be understandable.
   (i) Dijstra algoritm can be applied to any arbitrary graph.
   (j) The size of the minimal cycle basis for a given graph G=(V, E) is |V|-1.

3. (20 points) (a) Derive the best case, worst case and average case time complexity for the selection sort algorithm on n elements.

   (5 points) (b) Illustrate the operation of selection sort on the array A=[35, 5, 76, 1, 60, 10, 9, 16, 48, 18].

4. Given the following list: 14, 15, 5, 9, 8, 3, 19, 4
   (5 points) (a)Please construct a binary search tree for the sequence.
   (10 points) (b)Construct an AVL tree for the sequence.
   (10 points) (c)Construct a heap tree (note, the root has the maximum key) for the sequence.

國立雲林科技大學
99 學年度研究所博士班招生考試試題

所別：工程科技研究所
科目：工程數學（3）

1. (25 %) A consumer products company is formulating a new shampoo and is interested in foam height (in millimeters). Foam height is approximately normally distributed and has a standard deviation of 20 millimeters. The company wishes to test H_0: $\mu = 175$ millimeters versus H_1: $\mu > 175$ millimeters, using the results of $n = 10$ samples.
   (a) Find the type I error probability if the critical region is $\bar{x} > 185$. (10%)
   (b) Find the power of the test if the true mean foam height is 195 millimeters?(15%)

2. (10 %) Two chemical companies can supply a raw material. The concentration of a particular element in this material is important. The mean concentration for both suppliers is the same, but we suspect that the variability in concentration may differ between the two companies. The standard deviation of concentration in a random sample of $n_1 = 10$ batches produced by company 1 is $s_1 = 4.7$ grams per liter, while for company 2, a random sample of $n_2 = 16$ batches yields $s_2 = 5.8$ grams per liter. Is there sufficient evidence to conclude that the two population variances differ? Use $\alpha = 0.05$. (10%)

3. (15 %) The fraction of defective integrated circuits produced in a photolithography process is being studied. A random sample of 300 circuits is tested, revealing 13 defectives. Find a 95% two-sided CI on the fraction of defective circuits produced by this particular tool.

4. (15 %) 解 $(2x+1)^2 y'' - 2(2x+1)y' - 12y = 4x$

5. (15 %)試求下列 ODE 之解： $y'' + \dfrac{2}{x}y' + \dfrac{1}{x^4}y = \dfrac{2x^2+1}{x^6}$

6. (20 %) 設有二彈簧串連懸掛二法碼，如下圖所示。設彈簧常數分別爲 k_1、k_2，重量不計，法碼質量分別爲 m_1、m_2，在自然平衡位置時，伸長與重量達到靜力平衡，位移設定爲零，如下圖(a)所示。若不考慮阻尼力及其他驅動力，當施以一外力使後隨即釋放，彈簧即開始作簡諧運動，試寫出任一時間下個別彈簧伸長量 $x_1(t)$、$x_2(t)$隨時間變化之微分方程式(如圖(c))。(設 t=0 時，其伸長量分別爲 $x_1(0)$及 $x_2(0)$，如圖(b))

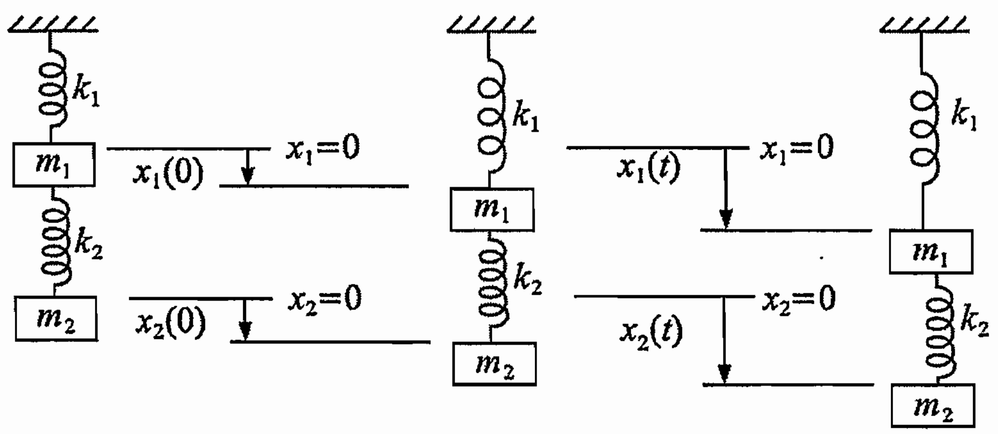

(a) (b) (c)

國立雲林科技大學
99 學年度博士班招生考試試題

所別：工程科技研究所、電子工程系
科目：工程數學 (2)

1. Choose a constant α so that the differential equation is exact, then produce a potential function and obtain the general solution. (15%)

   $3x^2 + xy^\alpha - x^2 y^{\alpha-1} y' = 0$

2. Find the general solution of the differential equation, using any method. (15%)

   $x^2 y'' + 3xy' + y = 9x^2 + 8x + 5$

3. Solve $y'' + 2y' + 2y = \delta(t-3)$; $y(0) = y'(0) = 0$ (10%)

4. If $f(t) = \cos t + e^{-2t} \int_0^t f(\alpha) e^{2\alpha} d\alpha$，find $f(t)$ (10%)

5. Solve the O.D.E. $x'' - 4x' + 3x = e^t$. (15%)

6. Suppose that the temperature $T(K)$ at the point (x, y, z) is given by $T = x^2 - y^2 - xyz + 273$; then in which direction is temperature increasing most rapidly at the point (1, 2, 3), and what is the rate? (20%)

7. Find the eigenvalues and eigenvectors of matrix

$$A = \begin{pmatrix} 5 & 8 & 16 \\ 4 & 1 & 8 \\ -4 & -4 & -11 \end{pmatrix}$$

(15%)

國立雲林科技大學
99學年度博士班招生考試試題

所別：工程科技研究所
科目：工程數學 (1)

本試題共 7 題，共計 100 分，請依題號作答並將答案寫在答案卷上，違者不予計分。

1. In each of problems (1) through (2). Find the Laplace transform of the function.
   (1) $\cos(t)-\sin(t)$; (2) $t^3-3t+\cos(4t)$ (10%)

2. In each of problems (1) through (2). Find the inverse Laplace transform of the function. (10%)
   (1) $\dfrac{2s-5}{s^2+6s}$; (2) $\dfrac{1}{s-4}-\dfrac{6}{(s-4)^2}$

3. To solve the initial value problem. (10%)
   $x^2y''+2xy'-6y=0 : y(1)=3, y'(1)=1$

4. To solve the differential equation. (10%)
   $e^x\sin(y)-2x+\left(e^x\cos(y)+1\right)y'=0$

5. To find the eigenvalues of $A=\begin{pmatrix}1 & -1 & 0\\ 0 & 1 & 1\\ 0 & 0 & -1\end{pmatrix}$. (10%)

6. (1) Find the Fourier transform of $f(t)=te^{-|t|}$; $F(\omega)=?$ (10%)

   (2) Find the inverse Fourier transform of $F(\omega)=\dfrac{1}{(1+\omega^2)(4+\omega^2)}$; $f(t)=?$ (10%)

7. Let $A=\begin{bmatrix}3 & 3\\ 1 & 5\end{bmatrix}$, $X=\begin{bmatrix}x_1\\ x_2\end{bmatrix}$, $X'=\begin{bmatrix}dx_1/dt\\ dx_2/dt\end{bmatrix}$ (本題共 30 分)
   (1) find the determinant of A, $|A|=?$ (5%)
   (2) find the eigenvalues and eigenvectors of the matrix A, (5%)
   (3) P is a matrix having the eigenvectors as columns, find P and P^{-1}, then diagonalize the matrix A. (5%)
   (4) find a fundamental matrix, $\Omega(t)$, for the system $X'=AX$, (5%)
   (5) find the general solution of $X'=AX$ by matrix methods. (10%)

國立雲林科技大學
99 學年度博士班招生考試試題
所別：工程科技研究所
科目：營建工程文獻評論

請從以下所附 A 題或 B 題，【A 題第 1 至 8 頁（Title: Improving Column Confinement）、B 題第 9 至 17 頁（Title: Near-Fault Ground Motion Effects on Reinforced Concrete Bridge Columns），考題總共爲 17 頁）】，選讀其中之一題，並針對所選讀之附件回答所對應之問題。請清楚標明所選讀之附件編號。

A 題：請說明本篇文獻之：1.背景與目的（25%）、2.內容與方法（25%）、3.比較與總結（25%）、4.缺點與限制（25%）。

Improving Column Confinement

Part 1: Assessment of design provisions

BY KENNETH J. ELWOOD, JOE MAFFEI, KEVIN A. RIEDERER, AND KARL TELLEEN

Providing transverse reinforcement in columns in the form of ties, hoops, or spirals is recognized as critically important for buildings that need to survive strong earthquakes. Transverse reinforcement is needed for any column—whether part of a moment frame or the gravity system—that must deform laterally under earthquake actions.

For flexure-governed columns, confinement provisions in the current ACI 318-08, "Building Code Requirements for Structural Concrete"[1] do not provide a consistent level of safety against deformation and damage associated with flexural yielding during earthquakes.[2] Potential replacement provisions are currently being discussed in Subcommittee H, Seismic Provisions, of Committee 318. In two parts, this article reviews confinement provisions from researchers and other building codes, compares the provisions with test data from 145 columns, and provides our recommendations for a confinement equation suitable for use in the ACI 318 Building Code.

PURPOSE OF TRANSVERSE REINFORCEMENT

In concrete columns, transverse reinforcement serves four functions, all of which are of magnified importance for cyclic post-yield behavior such as occurs in earthquakes. Transverse reinforcement:

- Resists shear forces. After diagonal shear cracking develops, ties or spirals act in tension as part of a diagonal truss mechanism;
- Clamps together lap splices. After splitting cracks form parallel to the splices, ties or spirals restrain slip between the spliced bars;
- Restrains the buckling of longitudinal reinforcement. After the concrete cover has spalled and, particularly, when the longitudinal reinforcement has yielded in tension and is subsequently cycled into compression, ties or spirals limit the unbraced length of the longitudinal bars; and
- Confines the concrete within the column core. After the concrete cover has spalled, ties or spirals allow the core concrete to sustain higher compression strains than would be possible without constraint.

While none of these functions are effective until the concrete has cracked or spalled, all are critical for ensuring that a column maintains lateral and vertical capacities under earthquake displacements in the post-yield range.

In rectangular columns, buckling of longitudinal bars is generally addressed by imposing limits on tie spacing s, and confinement of the concrete core is addressed by defining the minimum area of transverse reinforcement A_{sh} within s. The confining pressure is given by $A_{sh}f_{yt}/sb_c$, where f_{yt} is the yield strength of the transverse reinforcement and b_c is the width of the core measured to the outside of the confining bars.

CONFINEMENT PROVISIONS

Table 1 summarizes eight sets[1, 3-10] of confinement provisions for rectangular building columns. All of the provisions are intended for the design of structures in regions of high seismicity, and all can be expressed in terms of the confinement reinforcement ratio A_{sh}/sb_c in each transverse direction. Most of our discussions focus on the first four provisions listed in Table 1, designated ACI, CSA, NZS, and ITG, respectively. All provisions are discussed in more detail in References 2 and 5.

With the exception of ACI, the listed provisions were developed by placing limits on a deformation parameter

國立雲林科技大學
99 學年度博士班招生考試試題

所別：工程科技研究所
科目：營建工程文獻評論

TABLE 1:

SUMMARY OF CONFINEMENT EQUATIONS FOR RECTANGULAR REINFORCED CONCRETE BUILDING COLUMNS

Reference	$A_{sh}/sb_c =$	Deformation parameter	Notes
ACI 318-08[1]	$0.3\dfrac{f_c'}{f_{yt}}\left(\dfrac{A_g}{A_{ch}}-1\right)$	None	$f_{yt} \le 100$ ksi (689 MPa) $A_{sh}/sb_c \ge 0.09 f_c'/f_{yt}$
CSA A23.3-04[3]	$0.2 k_n k_p \dfrac{A_g}{A_{ch}}\dfrac{f_c'}{f_{yt}}$ where $k_n = n_l/(n_l-2)$ and $k_p = P/P_0$	μ_ϕ	$f_{yt} \le 500$ MPa $A_{sh}/sb_c \ge 0.09\ f_c'/f_{yt}$ based on Paultre and Légeron[12]
NZS 3101-06[4]	$\left(\dfrac{1.3-\rho_t m}{3.3}\dfrac{A_g}{A_{ch}}\dfrac{f_c'}{f_{yt}}\dfrac{P}{\phi f_c' A_g}\right)-0.006$ where $\phi = 0.85$	μ_ϕ	$\rho_t m \le 0.4$ ($m = f_{yl}/0.85 f_c'$) $A_g/A_{ch} \le 1.5$ $f_{yt} \le 800$ MPa based on Watson, Zahn, and Park* with $\mu_\phi = 20$
ITG 4.3R-07[5]	$\dfrac{b}{b_c}\left[0.35\dfrac{f_c'}{f_{yt}}\left(\dfrac{A_g}{A_{ch}}-1\right)\dfrac{1}{\sqrt{k_{ve}}}\dfrac{P_u}{A_g f_c'}\right]$ where $k_{ve} = \dfrac{0.15\, b_c}{\sqrt{s h_x}} \le 1.0$	δ	$P/A_g f_c' \ge 0.2$ $A_g/A_{ch} - 1 \ge 0.3$ based on Saatcioglu and Razvi[13] with $\delta = 0.025$
Sheikh and Khoury[6] Bayrak and Sheikh[7]	$0.3\dfrac{f_c'}{f_{yt}}\left(\dfrac{A_g}{A_{ch}}-1\right)(\alpha)\left(1+13\left(\dfrac{P}{P_0}\right)^5\right)\left(\dfrac{\mu_\phi^\gamma}{\beta}\right)$	μ_ϕ	α = configuration efficiency factor $f_c' \le 55$ MPa: $\beta = 29$, $\gamma = 1.15$ $f_c' > 55$ MPa: $\beta = 8.12$, $\gamma = 0.82$ $\mu_\phi = 16$ for high seismicity
Paulay and Priestley[8]	$k\dfrac{f_c'}{f_{yt}}\dfrac{A_g}{A_{ch}}\left(\dfrac{P}{A_g f_c'}-0.08\right)$	μ_ϕ	$k = 0.35$ for high ductility demand
Li and Park[9]	$\left(\dfrac{A_g}{A_{ch}}\dfrac{\mu_\phi-\Psi\rho_t m+22}{\lambda}\dfrac{f_c'}{f_{yt}}\dfrac{P}{\phi f_c' A_g}\right)-0.006$ where $\phi = 0.85$	μ_ϕ	$\mu_\phi = 20$ for high seismicity $\rho_t m \le 0.4$; $A_g/A_{ch} \le 1.5$ $f_{yt} < 500$ MPa and $f_c' < 70$ MPa: $\lambda = 117$, $\Psi = 33$ $f_{yt} < 500$ MPa and $f_c' \ge 70$ MPa: $\lambda = 0.05(f_c')^2 - 9.54 f_c' + 539.4$, $\Psi = 33$ $500 \le f_{yt} \le 900$ MPa: $\lambda = 91 - 0.1 f_c'$, $\Psi = 30$
Brachmann, Browning, and Matamoros[10]	$\left[\gamma \Big/ \left[1-0.8\left(\dfrac{P}{A_g f_c'}\right)\left(\dfrac{A_g}{A_{ch}}\right)\right]\right]^2 \dfrac{f_c'}{f_{yt}}$	δ	$\gamma = 0.2$ for regions of high seismicity $f_c' \le 116$ MPa $f_{yt} \le 830$ MPa

* Watson, S.; Zahn, F.A.; and Park. R., "Confining Reinforcement for Concrete Columns," *Journal of Structural Engineering*, ASCE. V. 120. No. 6, June 1994, pp. 1798-1824.

A_{ch} = cross-sectional area of structural member measured out-to-out of transverse reinforcement: A_g = gross area of column; A_{sh} = total cross-sectional area of transverse reinforcement (including crossties) within spacing s and perpendicular to dimension b_c; b_c = cross-sectional member core measured to outside edges of transverse reinforcement composing area A_{sh}; f_c' = specified cylinder strength of concrete; f_{yl} = specified yield strength of longitudinal reinforcement; f_{yt} = specified yield strength of transverse reinforcement; h_x = center-to-center spacing of longitudinal reinforcement laterally supported by corner of hoop or hook of crosstle; m = mechanical reinforcing ratio ($m = f_{yl}/0.85 f_c'$); n_l = number of longitudinal bars laterally supported by corner of hoop or hook of crosstie; P = axial compressive force on column; P_0 = nominal axial load strength at zero eccentricity ($P_0 = 0.85 f_c'(A_g - A_{st}) + A_{st} f_{yl}$); s = spacing of transverse reinforcement measured along longitudinal axis of member; ρ_t = total area of longitudinal reinforcement divided by A_g; ϕ = capacity reduction factor; μ_ϕ = curvature ductility ratio; and δ = drift ratio. Note: 1 ksi = 6.89 MPa.

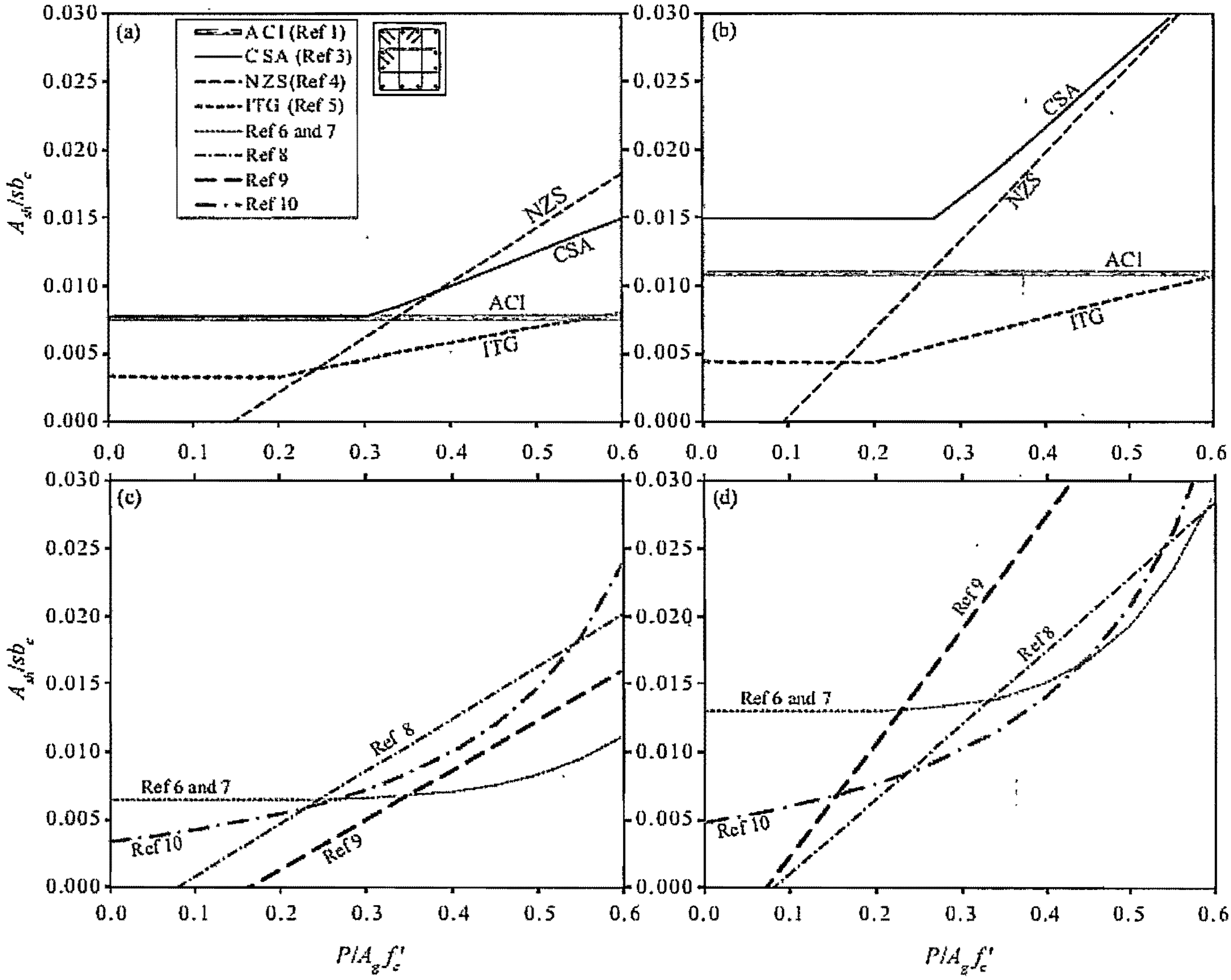

Fig. 1: Comparison of confinement provisions (see Table 1) applied to a 24 x 24 in. (600 x 600 mm) column with A_g/A_{ch} = 1.3 and 12 No. 9 (No. 30M) bars: (a) and (c) f_c' = 5 ksi and $f_{yt} = f_{yl}$ = 60 ksi; (b) and (d) f_c' = 12 ksi, f_{yt} = 100 ksi, and f_{yl} = 75 ksi. (1 ksi = 6.89 MPa)

at failure, where failure is defined as a specified reduction in lateral load resistance. The most commonly used deformation parameter is curvature ductility ratio μ_ϕ, the quotient of curvature at failure and curvature at first yield. Two of the provisions in Table 1, however, were developed using the drift ratio δ, the quotient of the interstory drift at failure and the story height. For any equation that explicitly incorporates a deformation parameter, its developers have recommended the value of the parameter to be used for design.

As Fig. 1 illustrates, ACI, CSA, NZS, and ITG can require widely differing amounts of confining reinforcement. When the axial load P exceeds $0.3A_g f_c'$ (where A_g is the gross cross-sectional area of the column and f_c' is the concrete cylinder strength) reinforcing amounts per ACI can be well below the values required per CSA and NZS. ITG consistently results in the lowest amount of confining reinforcement for the practical range of axial load, requiring less than 40% of the hoops and crossties specified by ACI for levels of P up to $0.2A_g f_c'$.

KEY PARAMETERS

Effective confining pressure

As with all the provisions in Table 1, provisions defining confining reinforcement are typically formulated to provide a confining pressure proportional to the concrete strength. The required A_{sh} is thus taken proportional to $sb_c f_c'/f_{yt}$. Based on assumptions of how much strain will occur in transverse reinforcement when the concrete dilates, several confinement provisions also place limits on the value of f_{yt} that can be used in calculations. For the provisions considered, limits on f_{yt} vary from 70 to 116 ksi (485 to 800 MPa). ACI limits f_{yt} to 100 ksi (690 MPa) (Table 1).

Axial load

The ability of the concrete core to sustain compressive strains tends to increase with confinement pressure. Compressive strains associated with lateral deformation are additive to the strains associated with axial load, so it follows that confinement reinforcement should be increased with axial load to ensure consistent lateral deformation capacity.

It should be noted that in columns with low axial load, deformation from bar slip within beam-column joints can contribute significantly to the lateral deformation of the column.[11] Lateral deformations associated with bar slip do not depend on confinement of the column core and, hence, provide additional deformation capacity to columns with low axial loads without the need for additional confining reinforcement. This is an additional reason why columns with low axial loads may require less confinement than those with high axial loads.

With one exception (ACI), the confinement provisions listed in Table 1 include the effect of axial load, normally by including the quotient of P and an index axial strength. This index strength is typically $A_g f_c'$, but Reference 12 uses $(A_g - A_s)f_c' + A_s f_{yl}$ while References 6, 7, and 13 use $0.85(A_g - A_s)f_c' + A_s f_{yl}$, where A_s and f_{yl} are the area and yield strength of the longitudinal reinforcement, respectively. Including an $A_s f_{yl}$ term allows somewhat reduced confinement reinforcement levels for columns with high percentages of longitudinal reinforcement, and it has also been shown to provide better correlation to ultimate curvature ductility capacity.[6,12] It's not entirely clear, however, why the amount of longitudinal reinforcement should be a beneficial variable—arrangement and spacing of longitudinal bars may be more important factors. We recommend using $A_g f_c'$ for its simplicity for the design process; adding an $A_s f_{yl}$ term does not seem to change the required confinement enough to warrant its inclusion.

CSA, NZS, and ITG are based on the assumption that the required

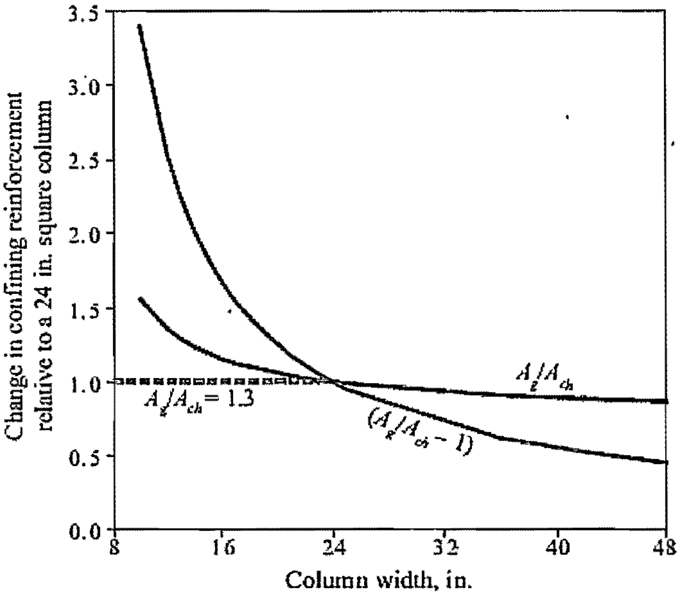

Fig. 2: Change in required confining reinforcement due to change in square column width (1 in. = 25.4 mm)

TABLE 2:
PARAMETER RANGES FOR PEER COLUMN DATABASE[15]

Parameter	Value		
	Minimum	Maximum	Average
f_{yt}, ksi (MPa)	36 (255)	200 (1420)	80 (550)
f_c', ksi (MPa)	3 (20.2)	17 (118.0)	8.6 (60.4)
s, in. (mm)	1 (25.4)	9 (229)	3 (77.5)
A_{sh}/sb_c, %	0.11	3.43	1.14
A_{sh}/A_g, %	1.01	6.03	2.37
A_g, in.^{2} (mm^2)	36 (23,200)	558 (360,000)	143 (92,500)
P/A_gf_c'	0.00	0.80	0.28

confinement pressure is directly proportional to P, but they take different approaches to ensuring columns with low axial load receive a minimum level of confinement. CSA is similar to ACI, with a minimum limit of $0.09f_c'/f_{yt}$ on A_{sh}/sb_c. NZS approaches $A_{sh}/sb_c = 0$ at $P \cong 0.1A_gf_c'$, but it relies on the requirements for bar buckling restraint and shear reinforcement to ensure sufficient transverse reinforcement at low axial loads. ITG limits the value of P used in calculation of confinement reinforcement to no less than $0.2A_gf_c'$.

Unconfined cover concrete

Concrete outside the core of a column—the cover concrete—is unconfined and will begin to spall when axial load and lateral deformation cause the compressive strain to reach 0.003 to 0.005. After spalling, there is a loss of flexural strength. This loss will be more significant if the area of unconfined concrete is a larger proportion of the total concrete area.

Each of the confinement provisions addresses this effect using the ratio A_g/A_{ch}, where A_{ch} is the area of the confined core. ACI is based on the work of Richart, Brandtzaeg, and Brown,[14] from 1929, which was focused on the effect of confinement on concentric axial strength. Rather than considering the effect of A_g/A_{ch} on lateral deformation capacity, the ACI equation was set up to equate the concentric axial strength of the confined core after spalling, considering concrete strength increase due to confinement, to that of the gross section before spalling. This formulation leads to a factor of $(A_g/A_{ch} - 1)$ in the confinement equation. To ensure that large columns have sufficient confinement, A_g/A_{ch} is limited to no less than 1.3. The same approach was used in the development of ITG.[12]

CSA and NZS make A_{sh} directly proportional to A_g/A_{ch}. This has been confirmed to be appropriate using moment-curvature studies.[11] Figure 2 shows how the two formulations affect the required amount of confining reinforcement for a square column. The figure suggests that relative to A_g/A_{ch}, $(A_g/A_{ch} - 1)$ may overemphasize the importance of the unconfined concrete cover.

Longitudinal reinforcement amount and spacing

The amount and transverse support of longitudinal reinforcement can also influence the amount of confinement required to achieve adequate deformability. CSA, NZS, and ITG include the influence of longitudinal reinforcement on the required amount of confining steel. The approaches taken, however, and the resultant impact on the requirements, are different for each of the provisions.

NZS allows a decrease in the amount of confining steel with an increase in the longitudinal reinforcement ratio. CSA and ITG include a similar effect, with the reasoning that having more longitudinal bars, restrained by hoops or crossties, improves confinement effectiveness because the confined concrete arches horizontally between restrained longitudinal bars. CSA accounts for this by including a factor k_n, related to the number of longitudinal bars restrained by corners of hoops or hooks of seismic crossties n_l. ITG accounts for this by using a

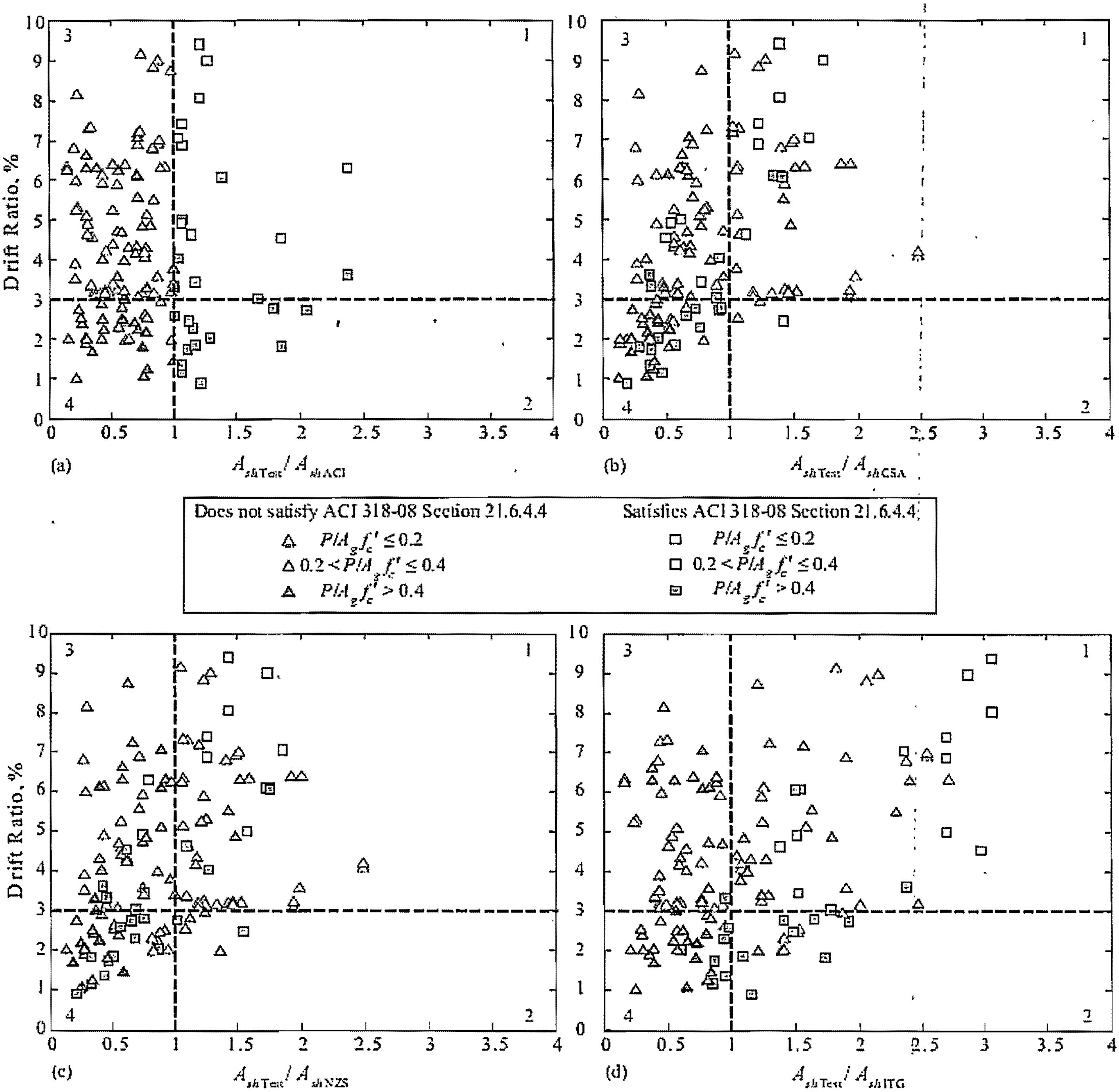

Fig. 3: Drift ratio capacity versus confinement provisions for rectangular columns: (a) ACI; (b) CSA; (c) NZS; and (d) ITG

factor that includes the horizontal spacing of restrained longitudinal bars h_x.

The factors related to the number or spacing of longitudinal bars as used in CSA and ITG account for an effect that seems at least moderately important in determining confinement effectiveness. As will be discussed in Part 2 of this article, the k_n factor used in CSA can be used to encourage good column detailing, both for confinement and the restraint of bar buckling.

EVALUATION OF CONFINEMENT PROVISIONS

Data and criteria

We evaluated the confinement provisions for rectangular columns using the PEER Structural Performance database.[15] Columns with nontypical or unknown properties, anomalous testing procedures, nonflexural failure modes, or not satisfying the ACI 318-08 minimum tie spacing of six longitudinal bar diameters (related to bar buckling) were removed. Although not all of the selected columns satisfy every requirement of ACI 318-08, each was judged to satisfy its *intent*, that is, to ensure flexural hinging prior to shear failure. Of the 301 rectangular columns in the database, 145 were suitable for comparisons. The measured drift ratio at a 20% reduction in the lateral force resistance (corrected for P-delta effects), provided by Reference 16, was used to assess the deformation capacity of the column specimens. Table 2 summarizes the range of key parameters found in the rectangular column database used for this study.

Although the provisions in Table 1 were developed based on different deformation parameters, a consistent performance measure is required to enable all to be compared against each other. Drift capacity was selected for several reasons: (1) this quantity is routinely reported for all test specimens, while the curvature ductility capacity is not; (2) it does not depend on the definition of yield displacement or yield curvature; and (3) the drift capacity can be directly related to drift limits specified in building codes.

We use 3% drift as a performance target in evaluating confinement provisions relative to test data. This corresponds to the largest permissible Maximum Considered Earthquake drift demand implied by U.S. building codes.[17] Maximum Considered demands are 1.5 times Design Basis demands, for which a 2% drift limit is specified for the types of buildings that are likely to contain concrete columns. Reference 2 evaluates the confinement provisions for a range of drift targets below and above 3% with similar conclusions to those reached in the following discussions.

Drift ratio capacity plots

Figure 3 shows column drift ratio capacities as functions of confinement provisions. The performance target is shown as a horizontal line at a 3% drift ratio. For an ideal confinement provision, all of the data would appear in the upper-right quadrant (Quadrant 1) and in the lower-left quadrant (Quadrant 4). Data in Quadrant 1 represent columns with confinement reinforcing exceeding that required by the considered provision but with drift capacities equal to or greater than the performance target. Data in Quadrant 4 represent columns with less confinement reinforcing than that required by the considered provision but with drift capacities less than the performance target. Data appearing in the upper-left quadrant (Quadrant 3) represent columns with less confinement reinforcing than that required by the provision but exhibiting a drift capacity exceeding the target, thus indicating that the provisions may be considered overly conservative in such cases. In contrast, data in the bottom-right quadrant (Quadrant 2) represent columns with more confinement reinforcing than required by the provision but exhibiting drift capacity below the target, thus indicating that the provisions may be considered unconservative for these cases.

The drift ratio capacity plots for ACI, CSA, NZS, and ITG are shown in Fig. 3(a), (b), (c), and (d), respectively. To avoid unrealistically low confinement requirements for NZS, a minimum confinement limit ($A_{sh,min} = 0.09 s b_c f_c'/f_{yt}$) was applied in Fig. 3(c). It should be noted that this approach could potentially result in overestimating the degree of conservatism provided by the NZS equation. The shape of the data points in Fig. 3 indicate whether or not the test column complied with ACI provisions, and the shading of the data points indicates the level of axial load used during testing.

ACI performance

Compared with ACI (Fig. 3(a)), a general trend of increasing drift capacity with an increase in the amount of confinement (relative to that suggested by the confinement equation) is more apparent in the CSA, NZS, and ITG plots (Fig. 3(b), (c), and (d), respectively). CSA provides a significant reduction in the number of "unconservative" data points (in Quadrant 2) compared with ACI. For ITG, 14 data points fall in the unconservative Quadrant 2, compared with 13 data points for ACI. All of the equations have fewer "overconservative" data points in Quadrant 3 compared with the ACI equation.

For ACI, all but one of the columns in Quadrant 2 of Fig. 3(a) were tested with $P/A_g f_c' \geq 0.4$. In contrast, only four of the 82 columns in Quadrant 3, where ACI is conservative, were tested with $P/A_g f_c' \geq 0.4$. This confirms that the most important change needed in the ACI confinement requirements is to have confinement reinforcement depend on axial load. To address this need, and considering the discussion of key parameters presented previously, Part 2 of this article proposes a new confinement provision for ACI 318.

Acknowledgments

The supporting research for this article was funded by the Portland Cement Association through the Education Foundation Research Fellowship program. This study was initiated on behalf of Joint ACI-ASCE Committee 441, Reinforced Concrete Columns. The quality of the study benefited from several discussions with committee members; this input is gratefully acknowledged. The authors are indebted to a committee of the Structural Engineers Association of California, chaired by Nicolas Rodrigues, which evaluated designs resulting from the various confinement equations, and to Zahra Riahi for her review of the study.

References

1. ACI Committee 318, "Building Code Requirements for Structural Concrete (ACI 318-08) and Commentary," American Concrete Institute, Farmington Hills, MI, 2008, 473 pp.

2. Riederer, K.A., "Assessment of Confinement Models for Reinforced Concrete Columns Subjected to Seismic Loading," The University of British Columbia, Vancouver, BC, Canada, Dec. 2006, 211 pp.

3. Canadian Standards Association, "Design of Concrete Structures," CSA A23.3-04, Mississauga, ON, Canada, 2004, 258 pp.

4. Standards Association of New Zealand, "Concrete Design Standard, NZS3101:2006, Part 1" and "Commentary on the Concrete Design Standard, NZS 3101:2006, Part 2," Wellington, New Zealand, 2006, pp. 646.

5. ACI Innovation Task Group 4, "Report on Structural Design and Detailing for High-Strength Concrete in Moderate to High Seismic Applications (ITG-4.3R-07)," American Concrete Institute, Farmington Hills, MI, 2007, 66 pp.

6. Sheikh, S.A., and Khoury, S.S., "A Performance-Based Approach for the Design of Confining Steel in Tied Columns," *ACI Structural Journal*, V. 94, No. 4, July-Aug. 1997, pp. 421-432.

7. Bayrak, O., and Sheikh, S., "Confinement Reinforcement Design Considerations for Ductile HSC Columns," *Journal of Structural Engineering*, V. 124, No. 9, 1998, pp. 999-1010.

8. Paulay, T., and Priestly, M.J.N., *Seismic Design of Reinforced Concrete and Masonry Buildings*, John Wiley & Sons, Inc., New York, NY, 1992, 768 pp.

9. Li, B., and Park, R., "Confining Reinforcement for High-Strength Concrete Columns," *ACI Structural Journal*, V. 101, No. 3, May-June 2004, pp. 314-324.

10. Brachmann, I.; Browning, J.; and Matamoros, A., "Relationships between Drift and Confinement in Reinforced Concrete Columns under Cyclic Loading," *Paper* No. 2531, 13th World Conference on Earthquake Engineering, Vancouver, BC, Canada, 2004.

11. Elwood, K.J., and Eberhard, M.O., "Effective Stiffness of Reinforced Concrete Columns," *ACI Structural Journal*, V. 106, No. 4, July-Aug. 2009, pp. 476-484.

12. Paultre, P., and Légeron, F., "Confinement Reinforcement Design for Reinforced Concrete Columns," *Journal of Structural Engineering*, ASCE, V. 134, No. 5, 2008, pp. 738-749.

13. Saatcioglu, M., and Razvi, S.R., "Displacement-Based Design of Reinforced Concrete Columns for Confinement," *ACI Structural Journal*, V. 99, No. 1, Jan.-Feb. 2002, pp. 3-11.

14. Richart, R.D.; Brandtzaeg, A.; and Brown, R.L., "The Failure of Plain and Spiral Reinforced Concrete in Compression," *Engineering Experiment Station Bulletin*, No. 190, University of Illinois, Urbana, IL, 1929.

15. Berry, M.; Parrish, M.; and Eberhard, M., "PEER Structural Performance Database User's Manual (Version 1.0)," 2004, http://maximus.ce.washington.edu/-peera1/.

16. Camarillo, H.R., "Evaluation of Shear Strength Methodologies for Reinforced Concrete Columns," MS thesis, Department of Civil and Environmental Engineering, University of Washington, Seattle, WA, 2003.

17. ASCE/SEI, "Minimum Design Loads for Buildings and Other Structures," ASCE/SEI 7-05, American Society of Civil Engineers, Reston, VA, 2006, 388 pp.

Received and reviewed under Institute publication policies.

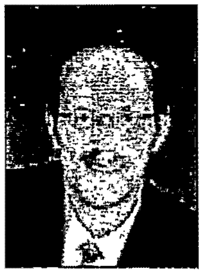

ACI member Kenneth J. Elwood is an Associate Professor at the University of British Columbia, Vancouver, BC, Canada. He is Chair of ACI Committee 369, Seismic Repair and Rehabilitation, and is a member of Joint ACI-ASCE Committee 441, Reinforced Concrete Columns. His research interests include the behavior and performance-based design of reinforced concrete structures under seismic loading. He received his PhD from the University of California, Berkeley, CA.

ACI member Joe Maffei is a Structural Engineer and Principal with Rutherford & Chekene consulting engineers in San Francisco, CA, where his practice includes a focus on the seismic design and retrofitting of concrete buildings. He is a member of ACI Committee 318H, Seismic Provisions. He is active in the Seismology Committee of the Structural Engineers Association of California (SEAOC) and serves as SEAOC's official liaison to ACI Committee 318H.

Kevin A. Riederer is a Structural Design Engineer on the International Team at Read Jones Christoffersen Ltd., in Vancouver, BC, Canada. Since joining the firm in 2006, his experience has included the structural design and analysis of concrete, steel, and wood frame buildings. He received his BSc in civil engineering from the University of Alberta and his MASc in civil engineering from the University of British Columbia.

Karl Telleen is a Senior Design Engineer with Rutherford & Chekene in San Francisco, CA, where his experience includes seismic design and retrofit of concrete and steel buildings. He received his BS from Princeton University and his MS from Stanford University. He is currently on leave from R&C, pursuing research at the École Polytechnique Fédérale de Lausanne on concrete structures.

國立雲林科技大學
99學年度博士班招生考試試題

所別：工程科技研究所
科目：營建工程文獻評論

B題：請說明本篇文獻之：1.背景與目的（25%）、2.內容與方法（25%）、3.比較與總結（25%）、4.缺點與限制（25%）。

Near-Fault Ground Motion Effects on Reinforced Concrete Bridge Columns

Vu Phan[1]; M. Saiid Saiidi, F.ASCE[2]; John Anderson[3]; and Hamid Ghasemi[4]

Abstract: Characteristics of near-fault ground motions warrant special consideration due to their severe and impulsive effects on structures. These characteristics are unique compared to far-field ground motions, upon which nearly all seismic design criteria are based. The objectives of this study were to explore the shake table response of reinforced concrete, to investigate near-fault ground motion effects on reinforced concrete bridge columns subjected to near-fault ground motions, and to provide a framework for the evaluation of bridge columns near active faults. Two large-scale columns were designed and tested under a near-fault ground motion on a shake table at the University of Nevada, Reno. One column represented the current California Department of Transportation far-field design, and the other was based on the American Association of Highway and Transportation Officials provisions. The most unique measured response characteristic in both columns was the large residual displacements even under moderate motions. A new hysteresis model was developed to capture this effect and was incorporated in an analytical model. Based on this finding, a framework for the evaluation of reinforced concrete bridge columns with respect to the control of residual displacement was proposed.

DOI: 10.1061/(ASCE)0733-9445(2007)133:7(982)

CE Database subject headings: Impulsive loads; Seismic design; Bridges, concrete; Concrete, reinforced; Hysteresis; Strain rate; Plastic hinges; Columns; Ground motion.

Introduction

Current seismic design criteria for reinforced concrete bridge columns, which were developed based on far-field ground motions, overlook the potentially adverse effects due to near-field forward directivity pulses. Because the majority of near-fault ground motions have been recorded only in recent years, the response on structures that these motions produce is not yet understood. A study was undertaken to investigate the unique effects that near-fault ground motions have on reinforced concrete bridge columns and to formulate a framework for the evaluation of single pier reinforced concrete bridge columns located near an active fault. To accomplish these goals, two cantilever columns were tested on a shake table using recorded near-fault ground motions. Based on the measured results and further analysis, inferences were made on the unique effects of an impulsive load on bridge columns and the effectiveness of current standard design provisions in the United States. A relatively simple evaluation procedure for bridge columns was then formulated as a preliminary model of what may be used in the design of bridge columns. It is to be noted that further testing and analysis of a much wider array of specimens and ground motions is required to generate a more comprehensive design criterion.

[1]Staff Engineer, CH2M HILL, 1100 112th Ave. NE, Suite 400, Bellevue, WA 98004. E-mail: vphan@ch2m.com

[2]Professor, Dept. of Civil and Environmental Engineering, Mail Stop 258, Univ. of Nevada at Reno, Reno, NV 89557. E-mail: saiidi@unr.edu

[3]Professor, Dept. of Geological Sciences and Engineering, Mail Stop 174, Univ. of Nevada at Reno, Reno NV 89557. E-mail: jga@unr.edu

[4]Research Engineer, Federal Highway Administration, Office of Infrastructure R&D, 6300 Georgetown Pike, McLean, VA 22101. E-mail: hamid.ghasemi@fhwa.dot.gov

Note. Associate Editor: Marvin W. Halling. Discussion open until December 1, 2007. Separate discussions must be submitted for individual papers. To extend the closing date by one month, a written request must be filed with the ASCE Managing Editor. The manuscript for this paper was submitted for review and possible publication on September 28, 2005; approved on December 8, 2006. This paper is part of the *Journal of Structural Engineering*, Vol. 133, No. 7, July 1, 2007. ©ASCE, ISSN 0733-9445/2007/7-982–989/$25.00.

Test Specimen Details

Two one-third scale bridge columns were tested on a shake table at the University of Nevada, Reno Large Scale Structures Laboratory. The two specimens were labeled NF-1 and NF-2, where "NF" stands for "near fault". Both columns were designed to behave as cantilever members and were representative of typical single column bridge piers in which the response is controlled by flexure.

The design of NF-1 was based on the 2004 Caltrans Seismic Design Criteria (SDC) version 1.3, but did not incorporate any of the current near-fault guidelines Caltrans provides (California Department of Transportation 2004). This made NF-1 nearly identical to a column, labeled 9F1, tested in the University of Nevada, Reno Large Scale Structures Laboratory during a previous study (Laplace 2005). The difference between the two specimens was that NF-1 was subjected to a near-fault impulsive ground motion (Rinaldi) but 9F1 was tested under an earthquake record that did not include forward directivity effects (El Centro 1940). The goal was to compare the effects of the two ground motions on similar columns.

The design of NF-2 was based on the AASHTO 2002 Standard Specifications for Highway Bridges (AASHTO 2002). Although the Caltrans SDC and AASHTO specifications differ in design approach, NF-1 and NF-2 were designed with the same geometric dimensions, soil type, and seismicity of the site. The purpose of testing NF-2 was to determine how a typical column designed to

Table 1. Specimen Details

Specimen	Column height (mm)	Column diameter (mm)	Longitudinal steel ratio (%)	Transverse steel ratio (%)	Axial load ratio (%)	Ground motion	Design criteria
NF-1	1829	406.4	2.0	0.92	8.0	Rinaldi	Caltrans SDC 2004
NF-2	1829	406.4	2.2	1.10	8.0	Rinaldi	AASHTO 2002
9F1	1829	406.4	2.0	0.92	8.0	El Centro	Caltrans Code 1992

AASHTO standards stands up to a near-fault ground motion, and to further enhance the understanding of near-fault ground motion effects on reinforced concrete columns.

Table 1 presents information for all three columns examined in this study. Note that the dimensions and reinforcement of NF-1 and 9F1 were identical, even though different versions of the Caltrans design criteria had been used. Measured reinforcement properties are listed in Table 2. Longitudinal steel diameter was 12.7 mm and transverse steel diameter was 6.35 mm for both specimens. During construction, concrete was poured in two stages: The footing and the column/head. Table 3 lists the measured concrete compressive strengths on the days of testing.

Shake Table Testing

The Rinaldi ground motion from the 1994 Northridge earthquake was selected for the testing of NF-1 and NF-2. This ground motion was chosen because the fault normal component displays a clear and definite pulse in the velocity history, is from a well-known earthquake, and is representative of western American soil characteristics. In addition, the Rinaldi ground motion had one of the highest peak ground velocities ever recorded, and preliminary analysis showed it generated large ductility demands compared to other near-fault ground motions. The Rinaldi ground motion serves as a satisfactory contrast to the El Centro motion, which was used for the 9F1 specimen test. From the 1940 Imperial Valley earthquake, the El Centro ground motion displayed no high amplitude velocity pulse due to forward directivity and its characteristics more closely resemble typical ground motions, upon which current seismic design criteria are based. The velocity histories of the Rinaldi ground motion and El Centro ground motion are presented in Figs. 1 and 2, respectively.

Extensive instrumentation was used to monitor the internal strains, curvatures, displacements, accelerations, and forces for each model. Fig. 3 shows the shake table test setup for NF-1. Both specimens were subjected to a series of Rinaldi ground motions in which the acceleration amplitude was scaled by an increasing factor in subsequent runs. The series started at a low amplitude motion, which then progressively increased after each run until failure occurred. Both columns were loaded with the fault normal component only. A total of 11 earthquake motion runs were applied on each of NF-1 and NF-2. The longitudinal bars ruptured at 135% of the original Rinaldi motion in both specimens. The peak ground acceleration for this run was 1.1*g*.

Virtually no damage was seen on the upper two-thirds of the column during the entire test sequence of both specimens. As expected for cantilever members, extensive damage was localized in the plastic hinge region near the base of the specimens. One side of each column suffered damage primarily from compression, which showed spalled concrete, buckled longitudinal bars, and extensive core damage. The other side experienced damage primarily from tension, which was seen through the extensive flexural cracking that grew wider with each subsequent run. Fig. 4 shows the test specimens at the completion of testing when failure occurred. Both columns experienced substantial permanent displacement as can be seen in the figure.

Response Comparison

Forces and Displacements

The cumulative measured force displacement hysteretic curves are shown in Figs. 5 and 6 for NF-1 and NF-2, respectively. The hysteretic data for both specimens show motion that is biased in one direction and becomes more prevalent in that direction after each subsequent run. This one-sided bias is attributed to the pulse in the near-fault Rinaldi ground motion. The high velocity pulse caused the specimens to swing in a whiplike fashion, generating high specimen displacements in one direction. When most of the earthquake energy is localized into a single short duration pulse, as with the Rinaldi record, the hysteretic response tends to be highly asymmetric. The Rinaldi ground motion has a peak velocity of 1,660 mm/s in one direction and a peak velocity pulse amplitude of 721 mm/s in the other direction. This asymmetry in the directivity pulse contributed to the shifted cycles in Figs. 5

Table 2. Measured Reinforcement Properties

Specimen	Yield stress (MPa)	Ultimate stress (MPa)
Longitudinal steel	469	644
Transverse steel	396	511

Table 3. Measured Concrete Compressive Strength

	Test day strength (MPa)	
Specimen	Footing	Column and Head
NF-1	38.7	41.3
NF-2	40.2	42.4

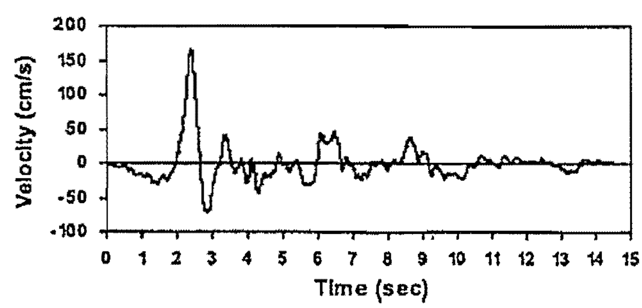

Fig. 1. Velocity history of fault normal component at Rinaldi Station

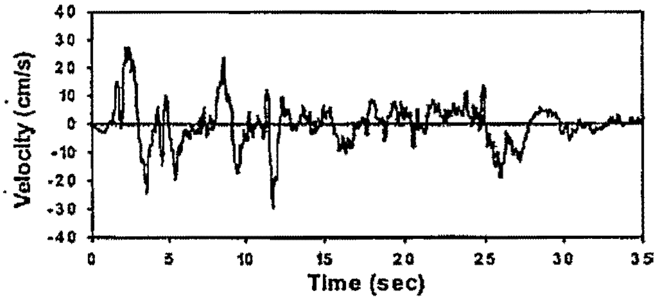

Fig. 2. Velocity history of fault normal component at El Centro Station

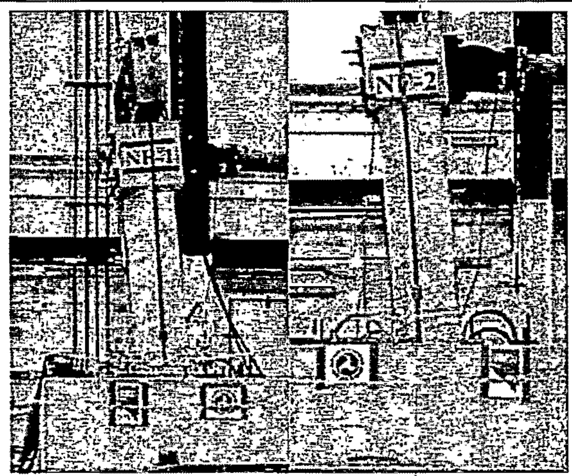

Fig. 4. Specimen NF-1 (a) and NF-2 (b) at completion of testing

and 6. The measured displacement ductility capacities were 11.1, 9.5, and 7.8 for NF-1, NF-2, and 9F1, respectively, based on elastoplastic idealizations of the envelope of the measured hysteresis curves.

Residual Displacements

The most unique measured response was the magnitude of the residual displacements in the responses of NF-1 and NF-2. Fig. 7 shows the measured residual drift ratio versus the peak ground acceleration (PGA). Residual drift ratio is defined as residual displacement divided by the length of the column. The data show that residual displacements in NF-1 and NF-2 were alarmingly high. For example, at PGA=0.5g, the residual drift ratio in both NF-1 and NF-2 exceeded 1%. As the PGA increased, the residual drifts in NF-1 and NF-2 also increased in an almost exponential manner. By comparison, the measured residual drifts in 9F1 were insignificant until the run with a PGA of 1.2g.

The high residual drifts in NF-1 and NF-2 are attributed to the unique characteristics of the near-fault ground motion. Note that 9F1 and NF-1 were nearly identical, yet NF-1 showed residual displacements up to 50 times higher than what was recorded for 9F1. The asymmetrical near-fault pulse can cause large displacements in one direction. Since near-fault ground motions tend to also have higher PGAs due to their proximity to the fault, the pulse can be strong enough to push a column far past the elastic range and not allow the column to return to its original position. The biased nature of the Rinaldi earthquake exacerbated the residual displacement with each subsequent run.

The large residual drift after even earthquakes with a moderate PGA presents several problems with respect to the bridge serviceability. Currently, there are no written guidelines for the design of reinforced concrete bridge columns with respect to control of residual displacement in either the AASHTO specifications or the Caltrans SDC. Although failure in the test specimens was defined as rupture in the reinforcement, in reality, a high residual displacement in a bridge column could indicate that the bridge is unsafe and must be closed to traffic even though the plastic hinge damage might be moderate. In Japan, reinforced concrete bridge columns with residual drift ratios of more than 1.75% were demolished and rebuilt after the Hyogo-ken Nanbu earthquake (Kawashima and MacRae 1998). This residual drift ratio limit was satisfied only up to run 6 with a PGA of only 0.5g in both NF-1 and NF-2.

NF-2 contained a 10% higher longitudinal steel ratio and a 20% more spiral steel ratio than those of NF-1. As a result, there was a 34% reduction in residual drift ratio in runs with a PGA of 0.25g and higher. Although an increase in reinforcement reduced the residual drift considerably, it would be premature to conclude that this is a general trend. This is because the combination of initial and effective stiffness, the yield level, the postyield stiffness, and the dominant period of the earthquake record could potentially alter this trend. Because of the importance of service-

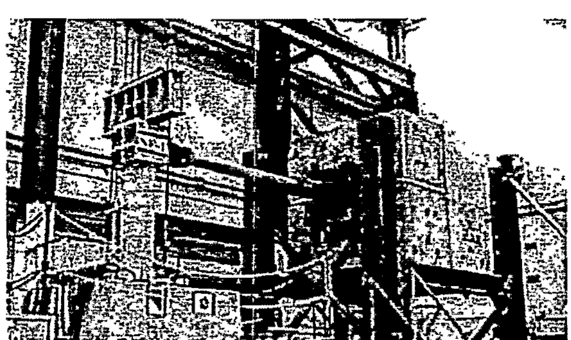

Fig. 3. Shake table setup for Specimen NF-1

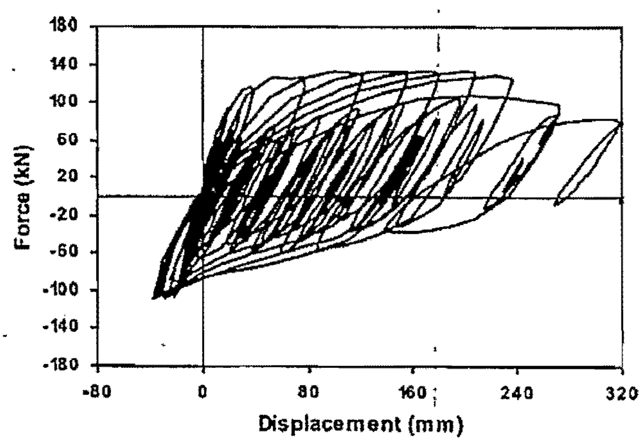

Fig. 5. Accumulated force displacement hysteresis for Specimen NF-1

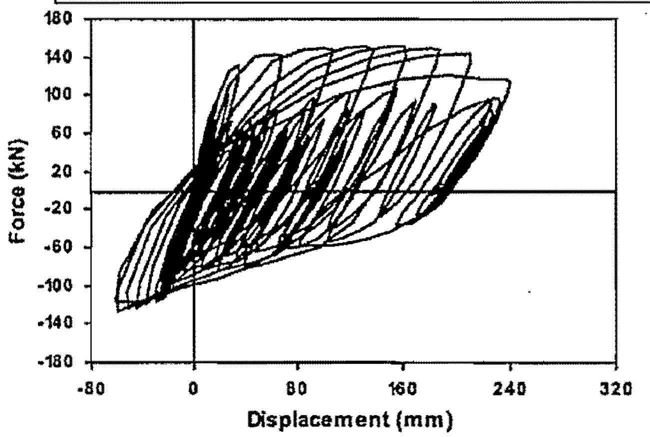

Fig. 6. Accumulated force displacement hysteresis for Specimen NF-2

ability after earthquake, a framework for the control of residual drift during the design of concrete bridge columns was developed and is presented in Appendix I.

Strain Rates and Plastic Hinge Lengths

The measured strain rates for NF-1, NF-2, and 9F1 are listed in Table 4. The strain rates presented are the peak instantaneous strain rate measured before yielding in tension or compression occurred. Some researchers have hypothesized that columns would experience a significantly higher strain rate from a near-fault ground motion due to the high velocity pulse (Gibson et al. 2002). Results show, however, that the measured peak strain rates for NF-1 and NF-2 were comparable to the measured values for 9F1.

Paulay and Priestley's equation for plastic hinge length (PHL) was used as the theoretical value for each specimen (Paulay and Priestley 1992). The theoretical value tends to be conservative for conventional reinforced concrete columns. For all three specimens examined in this study, the theoretical PHL was 286 mm. Concerns have been raised that current methods for calculating PHL may underestimate the actual value in structures subjected to near-fault ground motions (Hamilton et al. 2001). Table 5 lists the measured PHLs for NF-1, NF-2, and 9F1. The measured PHLs

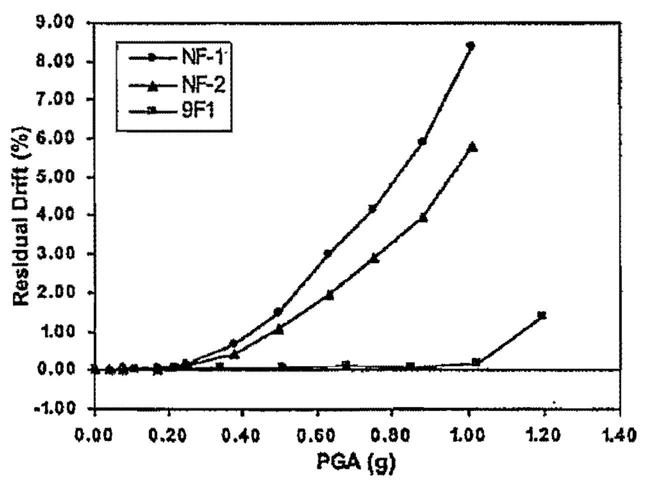

Fig. 7. Residual drift versus PGA

Table 4. Measured Peak Strain Rates

	Peak strain rate (microstrain/s)	
Specimen	Tension	Compression
NF-1	30,000	22,800
NF-2	33,400	18,500
9F1	32,900	19,200

were found based on the measured plastic displacements at the top of the columns, which is the same approach as that used by Paulay and Priestley (Paulay and Priestley 1992). The results in Table 5 show that the measured PHLs were longer than those predicted using Paulay and Priestley's equation. More importantly, the PHL under the Rinaldi record (NF-1) was comparable to that of the El Centro (9F1). Therefore, it appears that no modification to the plastic hinge equation is necessary to specifically account for the neal-fault effect on PHL.

To produce the critical strain rates and localized plastic hinge lengths, the pulse duration must be particularly short and the amplitude be high as with blast loading. The pulse of a blast load typically lasts for tenths of a second (Munshi 2004). Near fault directivity pulses normally have pulses with periods measured in whole seconds, however. Because of proximity, near fault ground motions carry a higher risk of producing large amplitudes, but typically have pulse durations too long to induce the strain rates and plastic hinge lengths that lead to brittle or early failure.

Dynamic Analysis

Initial dynamic analyses showed that existing hysteresis models, such as the Q-Hyst and Clough models, were not able to reproduce the measured residual displacements. Figs. 8 and 9 compare the measured displacement histories with those calculated using the Q-Hyst and Clough models for NF-1, respectively. Similar results were seen with NF-2. The lack of agreement is attributed to the fact that these models were developed based on column tests that were subjected to symmetric cyclic loading. The models assume that column has deteriorated and softened for loading in both directions. As a result, the load reversal stiffness is relatively small, thus facilitating the return of column to its baseline. The highly asymmetric loading in near-fault motions tends to soften the column only in one direction. The load reversal stiffness is hence relatively high, thus preventing the column from returning to its baseline. A new hysteresis model, called the O-Hyst model, was developed in this study to improve the correlation with the measured response. The "O" stands for "offset." Similar to the Q-Hyst and Clough models, the O-Hyst model operates on a bilinear primary curve (Fig. 8). Unloading after yield in O-Hyst (k3) takes into account stiffness degradation with the same equation as that used in the Q-Hyst model. The unique feature of the O-Hyst model is the use of an offset to define a change in the load reversal slope (Fig. 10). Instead of changing stiffness when load

Table 5. Measured Plastic Hinge Lengths

Specimen	Plastic hinge length (mm)	Ratio to diameter
NF-1	559	1.38
NF-2	433	1.07
9F1	432	1.06

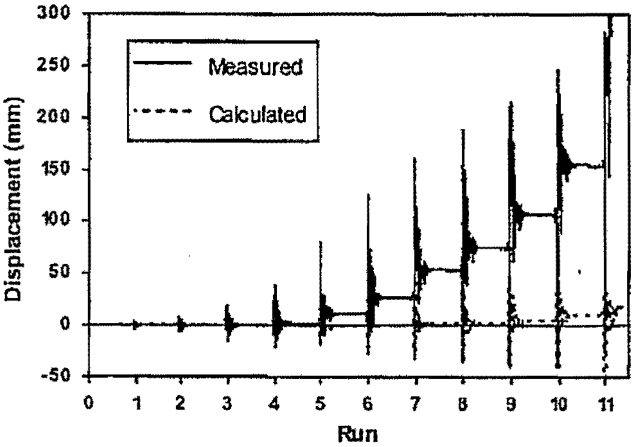

Fig. 8. Displacement history for NF-1 using Q-Hyst model

reversal occurs, as is the case for the Q-Hyst and Clough models, the unloading slope (lines k3 in Fig. 10) is maintained past the load reversal point until a predefined offset force value is reached.

The measured hysteresis curves for NF-1 and NF-2 corroborate the use of an offset value. In both specimens, the slope at load reversal did not change. Based on the measured data, an offset force of $F_y/3$ appeared to represent the point at which the stiffness changed. Once the offset force is reached, the path (k4 in Fig. 8) connects the offset point to a point on the bilinear backbone curve where the deformation is equal to the maximum displacement experienced in that direction. Therefore, the O-Hyst model takes into account differences in the maximum displacement in either direction, similar to the Clough model, and unlike the Q-Hyst model.

A nonlinear dynamic analysis program, DARC-O (Dynamic Analysis of Reinforced Concrete Columns with O-Hyst), was developed in this study. The program uses Newmark's Beta time-step method and was utilized for the dynamic analysis of single-degree-of-freedom systems. The calculated displacement histories for NF-1 and NF-2 are shown in Figs. 11 and 12, respectively. A close-up of the results for run 10 is also shown for each column. In general, the calculated and measured data correlated well during the first ten runs. The wave forms were similar and the residual displacements were estimated with a reasonably close agreement. During run 11, the longitudinal steel ruptured and major crushing in the concrete core was seen in both specimens.

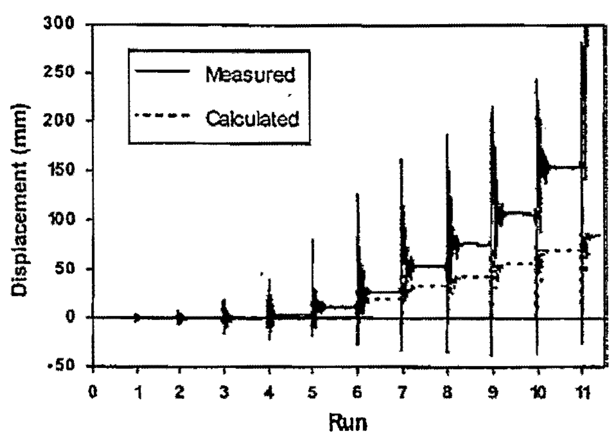

Fig. 9. Displacement history for NF-1 using Clough model

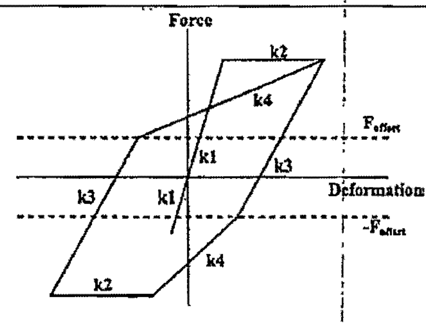

Fig. 10. O-Hyst model

DARC-O, however, does not take these events into account. Therefore, the deviation between the calculated and measured results for run 11 was high.

Framework for Near-Fault Earthquake Design

After a bridge undergoes major ground excitations, the columns may display large residual displacements, especially after a near-fault excitation. This was seen in the shake table tests conducted on NF-1 and NF-2. It is important that residual displacement be considered at the design stage to allow for maintaining a minimum level of service after the earthquake. Currently, there are no

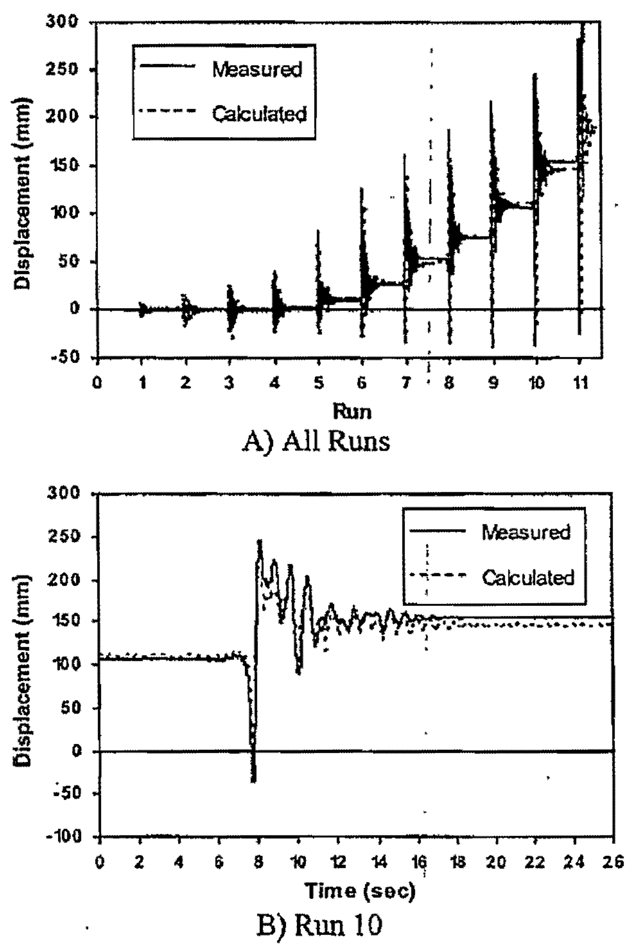

Fig. 11. Displacement history for NF-1 with O-Hyst model

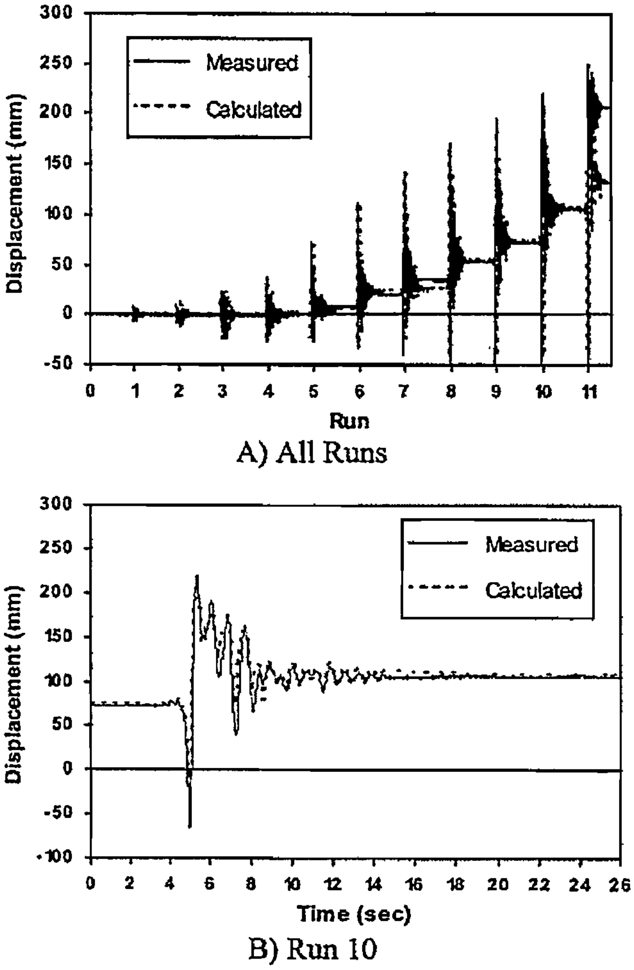

Fig. 12. Displacement history for NF-2 with O-Hyst model

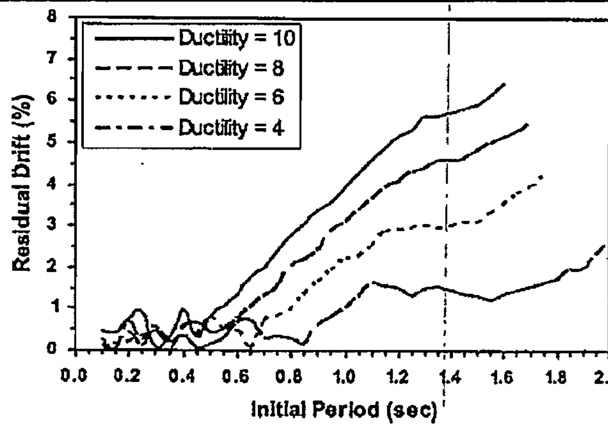

Fig. 13. Residual drift response spectra for composite source model (M_w=6.5 and stiff soil/soft rock)

written guidelines in either the AASHTO specifications or the Caltrans SDC for the design of reinforced concrete bridge columns with respect to the control of residual displacement. In addition, there are no guidelines to assess a damaged column with respect to residual displacement after an earthquake. A framework was developed in this study for the evaluation and design of reinforced concrete bridge columns taking into account the residual displacement effect.

Following major ground excitations, emergency vehicles may have to cross the damaged bridge. These emergency vehicles include fire trucks, ambulances, public utility assessment, repair units, etc. In the postearthquake time frame, when the all earthquake energy has dissipated, standing columns that display significant residual displacement present a risk for rescue teams that need to cross the damaged bridge. The additional live load of emergency vehicles can make the columns susceptible to collapse.

Instead of imposing an arbitrary residual drift limit on bridge columns, the objective of the proposed framework is to provide the user with a relatively simple method to determine the magnitude of live load that a column can safely resist before the reserve moment and rotational capacities are exceeded.

A cantilever single column reinforced concrete bridge pier was assumed. The procedure is considered to be a possible approach toward residual displacement consideration and not a full and final design recommendation. This is because not all components needed for a thorough and rational residual displacement design are currently available. Possible tentative recommendations are provided to make the framework complete with the understanding that future research will address the gaps. The development of the residual displacement spectra is presented in the next section and the design framework is presented in Appendix I.

Residual Drift Response Spectra

Residual drift response spectra were generated using program DARCO. Given an initial period and the expected displacement ductility demand for the column, the residual drift response spectra can be utilized to estimate the residual drift. Residual displacements were determined for ductilities of 4, 6, 8, and 10. For each ductility value, a residual drift response spectrum was generated. The curves were terminated when the residual drift exceeded 15%, or when the target ductility could not be achieved in the analysis.

The ground motions used to generate the residual displacement spectra included synthetic ground motion records. A synthetic ground motion is more suitable for use in design than an actual ground motion because it can incorporate general characteristics of a *collection* of earthquakes rather than a single earthquake. To generate synthetic records, the Composite Source Model program—developed at the University of Nevada, Reno—was utilized (Zeng et al. 1994). In the program, the fault and soil parameters are modeled and the locations of stations and the epicenter are selected. The program then simulates an earthquake and outputs ground motion acceleration histories at each station. To simulate the forward directivity pulse, fault rupture began at one end of the fault line and moved toward the station that was located at the other end. The station was positioned at 3.00 km perpendicular to the fault line. The synthetic records were chosen based on asymmetry in the velocity pulse, reasonable peak ground acceleration values, and the ability to produce high residual displacements in bridge columns. Fig. 13 presents the residual drift response spectra using the Composite Source Model for a 6.5 magnitude earthquake. More spectra were produced using other synthetic and actual ground motions (Phan et al. 2005). Results show that trends of the response spectra can vary considerably among different ground motions. To produce residual drift response spectra that are suitable for design, a collection of ground motions must be used so that an upper bound envelope could be established. Therefore, the residual drift response spectra used in Appendix I are preliminary and they are merely intended to demonstrate the application of the proposed framework.

Conclusions

The following conclusions were made based on the experimental and analytical results obtained in this study.

1. Near-fault earthquake records with forward directivity tend to contain an asymmetrical high amplitude velocity pulse that causes a whiplike behavior in columns and causes large displacements in one direction. This displacement is only partially recovered during the earthquake because the column stiffness upon load reversal is relatively large. As a result, significant residual displacement is developed.
2. Bridge column models designed based on the AASHTO and Caltrans guidelines for far-field earthquakes subjected to the Rinaldi record on a shake table experienced a residual drift ratio of 1% even when the PGA was normalized to 0.5g, which is considered to represent the PGA in a moderate earthquake.
3. The newly proposed O-Hyst hysteresis model led to calculated results that agreed well with the measured residual displacements. In contrast, the Q-Hyst and Clough hysteresis models were not successful in reproducing these displacements.
4. The plastic hinge length in columns subjected to near-fault ground motions is comparable to those of columns subjected to far-field motions. No modifications appear to be necessary to specifically account for the near-fault effect.
5. Strain rates induced by near-fault ground motions are comparable to strain rates induced by far-field ground motions. Pulse duration in near-fault excitations is generally not sufficiently short to produce significantly higher strain rates.
6. The proposed framework for the evaluation of residual displacements in the design and inspection of reinforced concrete bridge columns presents a relatively simple and rational process that allows for consideration of the unique effects of near-fault earthquakes.

Acknowledgments

The study presented in this paper was funded by the Federal Highway Administration. The writers are thankful to Patrick Laplace, Paul Lucas, and Hoon Choi of the UNR structures laboratory for their dedicated assistance in the course of shake table testing. Gratitude is also expressed to Aasha Pancha of the UNR Seismology program for developing the synthetic near-fault ground motion records.

Appendix I. Framework for Consideration of Residual Displacement

The following framework is tentatively proposed to address residual displacement in single reinforced concrete columns during design or as a tool to assess the safety of the bridge after earthquakes. Detailed description of the framework is presented in (Phan et al. 2005).

1. **Estimate residual drift of column**—Using a target ductility demand and residual drift spectra for earthquakes expected at the site, estimate the residual displacement and rotation.
2. **Estimate residual moment after earthquake**—After the earthquake, gravity loads and the P-Delta effect induce the following moments in the column:

$$M_{\text{postEQ}} = \Delta_{\text{residual}}\left(\text{DL}_{\text{superstructure}} + \frac{1}{2}\text{DL}_{\text{column}}\right) + M_g \quad (1)$$

3. **Estimate remaining moment capacity (RMC), M_{cap}**

$$M_{\text{cap}} = \alpha M_p \quad (2)$$

where α indicates the fraction of the plastic moment capacity, M_p, that the column can resist after the earthquake. There are no methods available to determine this fraction. The value of α was assumed to be a function of the expected displacement ductility, μ_{exp}

$$\alpha = 1.27 - 0.133\mu_{\text{exp}} \qquad \begin{matrix}\alpha \leqslant 1.0\\ \alpha \geqslant 0.20\end{matrix} \quad (3)$$

If M_{postEQ} is equal to or greater than M_{cap}, no live load can be applied to the column and the bridge would have to be redesigned to reduce residual displacements (or closed to traffic when the framework is used for evaluation of an existing bridge after the earthquake). Otherwise, continue with the procedure outlined next.

4. **Calculate reserve moment capacity, δM, and associated displacement, $\delta\Delta$**—The difference between the remaining capacity and the existing moment after the earthquake is δM. The lateral displacement, $\delta\Delta$, corresponding to δM is found based on the reserve force capacity, δF, and the estimated effective stiffness

$$\delta M = M_{\text{cap}} - M_{\text{postEQ}} \quad (4)$$

$$\delta F = \frac{\delta M}{L} \quad (5)$$

$$\delta\Delta = \frac{\delta F}{(k1/\mu_{\text{exp}})} \quad (6)$$

5. **Calculate allowable live load based on moment capacity**—The allowable live load after the earthquake, $\text{LL}_{\text{allowable}}$, is found from the following equation assuming that there is sufficient rotational ductility capacity

$$\text{LL}_{\text{allowable}} = \frac{M_{\text{postEQ}} + \delta M}{\Delta_{\text{residual}} + \delta\Delta} - \left(\text{DL}_{\text{superstructure}} + \frac{1}{2}\cdot\text{DL}_{\text{column}}\right) \quad (7)$$

6. **Check ultimate rotational capacity**—Assuming the column has already yielded

$$\delta\theta = \frac{\delta\Delta}{(L-(L_p/2))} \quad (8)$$

$$\theta = \theta_{\text{residual}} + \delta\theta \quad (9)$$

$$\theta \leqslant \theta_{\text{cap}} \quad (10)$$

Eq. (8) assumes that once the column has yielded, the PHL stays constant and curvature does not vary within the hinge zone. The ultimate rotation capacity, θ_{cap}, may be computed through a pushover analysis. If Eq. (10) is true, applying the live load determined from Eq. (7) is acceptable, and the remaining steps would not be necessary. Otherwise, a new lower allowable live load has to be found using the steps outlined next.

7. Calculate reserve rotational capacity

$$\delta\theta = \theta_{cap} - \theta_{residual} \quad (11)$$

8. Calculate reserve displacement capacity based on rotational capacity—Assuming the column has already yielded

$$\delta\Delta = \delta\theta\left(L - \frac{L_p}{2}\right) \quad (12)$$

9. Calculate associated moment based on rotational capacity

$$\delta F = \delta\Delta\left(\frac{k1}{\mu_{exp}}\right) \quad (13)$$

$$\delta M = \delta F \times L \quad (14)$$

10. Calculate final allowable live load—Use Eq. (7) to determine $LL_{allowable}$ with the new values computed based on rotational capacity. After the allowable live load has been calculated, the engineer can determine if emergency vehicles should be allowed on the bridge.

Appendix II. Design Example

The following values were based on the design of the NF-2 prototype: L=5486 mm; L_p=828 mm; $k1$=25.4 kN/mm; M_p=6,815,000 kN mm; DL=3203 kN; and θ_{cap}=0.0412 rad. For this example, an estimated maximum ductility of 6 is assumed. The initial period is 0.712 s.

The first step is to determine if there is any reserve moment so that additional live load can be applied. Assuming a 6.5 magnitude earthquake, a residual drift demand of 0.7% was obtained from Fig. 13. This corresponds to a displacement of 38.4 mm and rotation of 0.00757 rad. Neglecting gravity load moment, the moment after the earthquake using Eq. (1) is 123,000 kN mm. The moment reduction factor, α, is 0.472 using Eq. (3). The residual moment capacity can then be computed using Eq. (2) and is 3,217,000 kN mm. A reserve moment capacity of 3,094,000 kN mm is determined using Eq. (4). Since the reserve moment capacity is a positive number, there is moment capacity left to allow additional live load to be applied. The next step is to determine the amount of live load the column can support based on the reserve moment capacity. Using Eqs. (5) and (6), the reserve lateral force capacity and associated lateral displacement are 564 kN and 133 mm, respectively. The allowable live load based on moment capacity is 15,570 kN. If the allowable live load from Eq. (7) exceeds the live load the column was designed for, the design value should be used. Ambulances typically weigh around 46 kN. Fire trucks, however, can be 440 kN or more. At this point, the design is sufficient, but rotational capacity needs to be checked as well. If the rotational capacity is surpassed before the moment capacity, the allowable live load must be recalculated based on the reserve rotational capacity. The reserve rotational demand based on the moment capacity needed to allow the live load calculated in Eq. (7) is 0.0262 rad (Eq. (8)). The rotational demand is 0.0338 rad [Eq. (9)]. The rotational demand is less than the rotational capacity (0.0412 rad). Therefore, rotational capacity will not govern the amount of live load permitted on the column. Because allowable live load based on moment capacity was found to be sufficient, no changes are needed for the column design based on residual displacement. Had there been insufficient reserve capacity, the longitudinal and lateral reinforcement would need to be increased and the process be repeated until the allowable live load is adequate.

Notation

The following symbols are used in this paper:

DL_{column} = dead load of the column;
$DL_{superstructure}$ = tributary dead load of the superstructure;
$k1$ = initial (elastic) stiffness;
L = length of the column;
L_p = plastic hinge length of the column;
$LL_{allowable}$ = allowable post-earthquake live load;
M_{cap} = residual moment capacity;
M_g = gravity load moment;
M_p = plastic moment capacity;
M_{postEQ} = post-earthquake residual moment demand;
α = residual moment capacity factor;
$\Delta_{residual}$ = residual displacement;
$\delta F, \delta M, \delta\Delta, \delta\theta$ = reserve or associated force, moment, displacement, and rotation;
θ = rotational demand;
θ_{cap} = ultimate rotation capacity;
$\theta_{residual}$ = residual rotation of the column; and
μ_{exp} = estimated maximum column displacement ductility experienced under the earthquake.

References

American Association of State Highway and Transportation Officials. (2002). *LRFD bridge design specifications*, Washington, D.C.

California Department of Transportation. (2004). "Seismic design criteria." Sacramento, Calif.

Gibson, N., Filiatrault, A., and Ashford, S. (2002). "Impulsive seismic response of bridge column-cap beam joints." *ACI Struct. J.*, 99(6), 470–479.

Hamilton, C. H., Pardoen, G. C., Kazanjy, R. P., and Hose, Y. D. (2001). "Experimental and analytical assessment of simple bridge structures subjected to near-fault ground motions." *Proc., Int. Conf. of Engineering Mechnanics and Computation*, Univ. of Cape Town, Cape Town, South Africa.

Kawashima, K., MacRae, G. A., Hoshikuma, J., and Nagaya, K. (1998). "Residual displacement response spectrum and its application." *J. Struct. Eng.*, 124(5), 523–530.

Laplace, P. N., Sanders, D. H., Saiidi, M., Douglas, M. B., and El-Azazy, S. (2005). "Performance of concrete bridge columns under shake table excitation." *ACI Struct. J.*, 102(3), 438–444.

Munshi, J. (2004). "Seismic versus blast loading." *Concr. Int.*, 26(5), 58–64.

Paulay, T., and Priestley, M. J. N. (1992). "*Seismic design of reinforced concrete and masonry buildings.*" Wiley, N.Y.

Phan, V. T., Saiidi, S., and Anderson, J. (2005). "Near-fault (near-field) ground motion effects on reinforced concrete bridge columns." *Rep. No. CCEER-05-7*, Center of Civil Engineering Earthquake Research, Dept. of Civil Engineering, Univ. of Nevada, Reno, Nevada.

Zeng, Y., Anderson, J. G., and Yu, G. (1994). "A composite source model for computing realistic synthetic strong and ground motions." *Geophys. Res. Lett.*, 21(8), 725–728.